Available online at www.sciencedirect.com
ScienceDirect
Journal of Physics and Chemistry of Solids 67 (2006) 2550–2558
JOURNAL OF PHYSICS AND CHEMISTRY OF SOLIDS
www.elsevier.com/locate/jpcs

Synthesis and spectroscopic studies of iron (III) complex with a quinolone family member (pipemidic acid)

D. Skrzypek[a,*], B. Szymanska[a], Dimitra Kovala-Demertzi[b,*], Joanna Wiecek[b], E. Talik[a], Mavroudis A. Demertzis[b]

[a]*A. Chełkowski Institute of Physics, University of Silesia, Uniwersytecka 4, 40 007 Katowice, Poland*
[b]*Section of Inorganic and Analytical Chemistry, Department of Chemistry, University of Ioannina, Ioannina 45110, Greece*

Received 13 October 2005; received in revised form 14 July 2006; accepted 27 July 2006

Abstract

The interaction of iron (III) with pipemidic acid, Hpipem, afforded the complex [Fe (pipem) $(HO)_2$ $(H_2O)]_2$. The new complex has been characterised by elemental analyses, infra-red, EPR and XPS spectroscopies. The monoanion, pipem, exhibits O, O ligation through the carbonyl and carboxylato oxygen atoms. Six coordinate dimer distorted octahedral configuration has been proposed for [Fe (pipem) $(HO)_2$ $(H_2O)]_2$.

Keywords: A. Non-crystalline materials; B. Chemical synthesis; D. EPR

1. Introduction

Pipemidic acid (PPA-i.e., 8-methyl-5,8-dihydro-5-oxo-2-(1-piperazinyl)-pyrido[2,3-*d*]pyrimidine-6-carboxylic acid, Hpipem. $3H_2O$) is a quinolone derivative with the molecular structure shown in Fig. 1 [1]. It is well known for its antibacterial activity via inhibition of the synthesis of deoxyribonucleic acid (DNA). PPA is used in the treatment of urinary-tract infections [2].

Iron is an essential trace element for many biological functions, such as oxygen transport (through the haemoglobin); the synthesis of DNA, RNA and proteins; electron transport; cellular respiration; cell proliferation and differentiation; regulation of gene expression. It serves as a catalytic component in many enzymes [3].

Interactions of iron and others metalloelements with drugs administered for therapeutic purposes are a subject of considerable interest [2–5]. It is known, that some drugs work by chelation or inhibiting the activity of metalloenzymes. Therefore, metal ions might play a vital role during the biological process of drug utilisation in the body [2]. Yang et al studied complexes of PPA with some rare earth metals. The results suggested that metal ion coordination might be involved in the antibacterial activity of PPA [2]. Synthesis and characterisation of copper and manganese complexes of pipemidic acid have been referred [6].

In the present paper we report the EPR and XPS spectroscopic study of novel iron (III) complex of PPA. The analysis of electronic and magnetic properties is important to establish the structure of the active components of the pharmaceutical preparations.

2. Experimental procedure

2.1. General considerations

The reagents (Aldrich, Merck) were used as supplied, while the solvents were purified according to standard procedures. Pipemidic acid was a gift from Farmaceutici Damor S.p.A. C, H and N analyses were carried out by the microanalytical service of the University of Ioannina. Melting points were determined in open capillaries and are uncorrected. Infra-red and far-infra-red spectra were recorded on a Nicolet 55XC Fourier transform

*Corresponding authors. Tel./fax: +48 3225 884 31 (D. Skrzypek), Tel.: +32 6510 984 25; fax: +32 6510 987 91 (D. Kovala-Demertzi).
E-mail addresses: dskrzyp@us.edu.pl (D. Skrzypek), dkovala@cc.uoi.gr (D. Kovala-Demertzi).

0022-3697/$ - see front matter © 2006 Elsevier Ltd. All rights reserved.
doi:10.1016/j.jpcs.2006.07.013

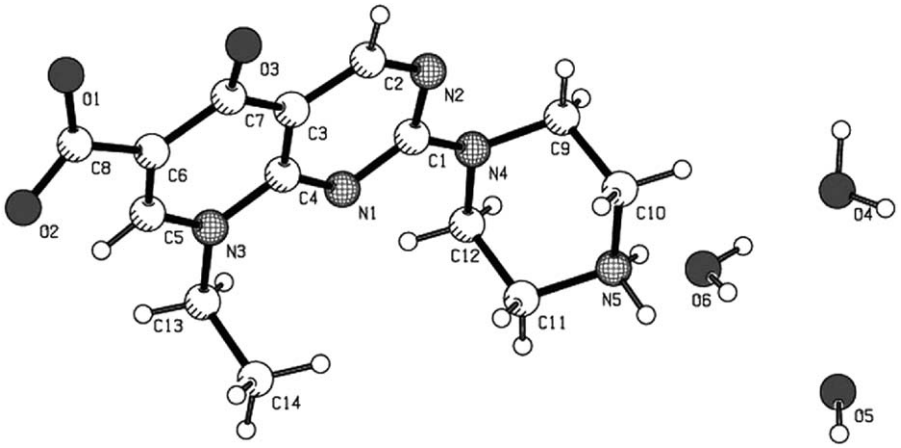

Fig. 1. The zwitterionic form of Hpipem $*3H_2O$ [1].

spectrophotometer using KBr pellets (4000–400 cm^{-1}) and nujol mulls dispersed between polyethylene discs (400–40 cm^{-1}). UV spectra were acquired with a JASCO V-570 spectrophotometer UV/VIS/NIR. The X-ray powder diffraction (XRD) analysis was carried out with the use of Siemens D5000 diffraction equipment. The filtered CuK_α radiation was selected and the scans were recorded in a (5–100°), 2θ range.

2.2. Synthesis of [Fe (pipem) $(HO)_2$ $(H_2O)]_2$

Complex A: a solution of $FeCl_3$ (0.0812 g, 0.5 mmol) in methanol (5 ml) was added to a solution of pipemidic acid (0.3030 g, 1 mmol) in methanol (10 ml). Drops of triethylamine ($N(eth)_3$) were added till the apparent pH value was ~7. The reaction mixture was stirred at room temperature for 2 h and cooled to 5 °C in a refrigerator for 4 h. The yellow powder was collected by filtration, washed with cold methanol and diethyl ether and dried in vacuo to afford [Fe (pipem) $(HO)_2$ $(H_2O)]_2$. Anal. Calc. for $C_{24}H_{20}FeN_5O_6$: C, 41.00; H, 4.91; N, 17.08; Found: C, 41.23; H, 5.00; N, 16.80%. IR (KBr, cm^{-1}): ν (OH), 3418 (br s); ν (NH), 2974 (m), ν (CH), 2818 (m); ν (CH_2), 2720 (m); ν (C═O), 1627 (s, br); ν_{asym} (COO), 1609; ν_{sym} (COO), 1362 (s); ν (C═N), 1531 (ms); ν (Fe–O–Fe), 620 (ms); ν ($F-O_{H_2O}$), 389 (s); ν ($Fe–O_{c=o}$), 319 (ms); ν ($Fe–O_{oco}$), 303 (m). UV–Vis (H_2O) λ/nm (ε/lit mol^{-1} cm^{-1}) 329 (12,000), 266 (46,000).

Attempts to synthesise the Fe (II) complex of pipemidic acid, under nitrogen, were unsuccessful. During synthetic process an oxidation takes place and instead of Fe (II), the same complex is obtained.

The compound studied in this work was used in the form of solid sample. The crystalline structure was investigated by powder X-ray diffraction. The X-ray diffraction pattern of Fe (III)–PPA complex in Fig. 2 indicates that this compound is poorly crystallised. EPR, IR, UV-Vis. and XPS spectroscopies have proved to be a powerful tool for identifying the coordination site, the oxidation and spin states of paramagnetic elements and the local order around the central metal ion.

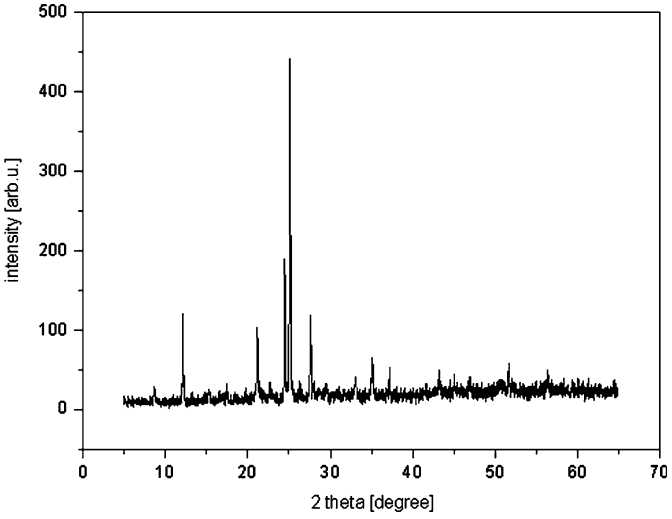

Fig. 2. X-ray powder diffraction pattern of the Fe (III)–pipemidic acid complex.

2.3. Methods

The EPR spectra were recorded on Radiopan SE/X spectrometer with TE_{102} rectangular cavity and 100 kHz field modulation, equipped with an Oxford Instruments ESR 910 helium flow cryostat. The microwave frequency was measured using Hewlett Packard 534 microwave frequency counter and the magnetic field strength was monitored by a NMR teslameter. The temperature dependence measurements were performed in the temperature range from 3 to 300 K. The EPR parameters were confirmed by simulation using Bruker-Symphonia software package.

The XPS spectra were obtained using a PHI 5700/660 Physical Electronics Photoelectron Spectrometer with monochromatized Al K_α X-ray radiation (1486.6 eV). The XPS spectra were calibrated using the Au $4f_{7/2}$ signal from an Au-foil whose binding energy is 84 eV. The pass energy value used for the high-resolution spectra acquisition together with the full-width at half-maximum height

(FWHM) obtained on a metallic sputtered Ag were 11.75 and 0.63 eV, respectively. So, the resolution value is around 0.7 eV. The compounds in powder form were mounted onto standard sample holder by means of double-sided adhesive carbon disc. The measurements were performed from a surface area of $800 \times 2000\,\mu m$ under UHV conditions, 10^{-8} Pa. In every case the neutraliser was used due to a charge effect that occurs for non-conducting samples. The binding energy was determined by reference to the C1s component from hydrocarbons at 284.5 eV [7]. The peak shapes were fitted after Shirley background subtraction, using the Gaussian–Lorenzian function.

3.Results. and discussion

3.1. IR spectra

The IR spectra of Hpipem.$3H_2O$ do not have a v (C═O) absorption according to the crystal structure of Hpipem, where the carboxylic group is deprotonated and the molecule exists in zwitterionic form [1]. It is known that ionic carboxylates [4] show no carbonyl stretching at about 1700 cm^{-1}, but have two characteristic bands in the range of 1650–1510 cm^{-1} and 1400–1280 cm^{-1} that could be assigned as v_{asym} and v_{sym} (COO) stretching vibrations. As the carboxyl hydrogen is more acidic than the amino hydrogen the deprotonation occurs in the carboxylic group. This is confirmed by the IR spectra of the complexes, showing the characteristic bands for the secondary amino groups and for the coordinated carboxylato group. The IR of Hpipem.$3H_2O$ and [Fe (pipem) $(HO)_2$ $(H_2O)]_2$ gave band at 3021, 2960 and 2974 and 2934 cm^{-1}, respectively attributable to intra- or intermolecular NH–O hydrogen bonds. A broad absorption at ~3400 cm^{-1} in the spectra of the complexes was attributed to the presence of coordinated water [8]. The v_{asym} (COO) and v_{sym} (COO) bands appear at 1609 and at 1362 cm^{-1}, respectively. The difference, $\Delta[v_{asym}$ (COO)-v_{sym} (COO)] between these frequencies is 247. This value is consistent with monodentate coordination of the carboxylato group [9]. The non-ligand band at 620 for [Fe (pipem) $(HO)_2$ $(H_2O)]_2$ is assigned to v (Fe–O–Fe) mode. The non-ligand bands at 391, 319 and 277 cm^{-1} are tentatively assigned to v ($F-O_{H_2O}$), v ($Fe-O_{c=o}$) and v ($Fe-O_{oco}$) modes, respectively [2]. These data indicate coordination through the oxygen atoms of the carboxylato group, carbonyl group and water molecule and no interaction between the endocyclic nitrogens (C═N) and metal ions.

3.2. EPR studies

Fig. 3 shows the EPR spectrum of Fe (III)–PPA complex recorded at a room temperature. There are some characteristic features, which imply the presence of more then one type of paramagnetic species in the sample. The observed spectrum is attributed to a combination of isolated paramagnetic ions in different environments and magnetically coupled Fe^{3+} ions.

A characteristic feature of the spectrum is the dominating absorption at $g_{eff} = 4.3$. This absorption is, as a rule, observed in Fe^{3+}-doped disordered media [10–12] and it is generally assigned to Fe^{3+} in a weak crystal field

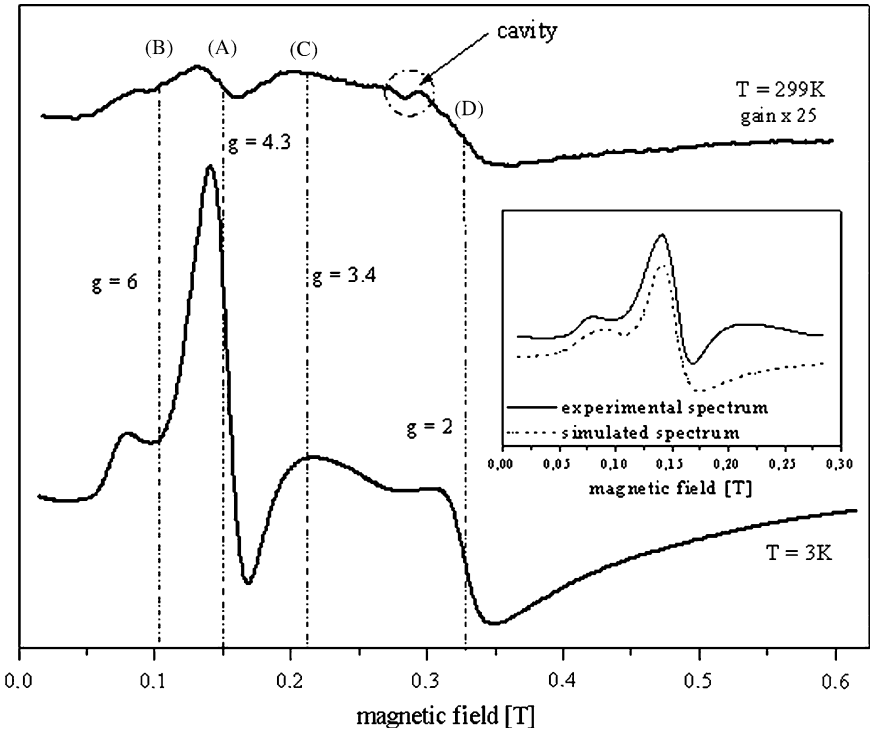

Fig. 3. The EPR spectra of solid ferric–PPA complex at a room temperature and at T = 3 K. The insert shows the low-field HS peaks and their simulation.

environment. In this system, the $^6A_1$ ground state is split into three Kramers doublets due to spin-orbit mixing with excited states. These doublets are split by an applied magnetic field and the near isotropic g-factor of 4.3 is assigned to a transition within one of them [11]. Many authors [13] have discussed the matter from different points of view. Kliava [10] analysed the EPR spectra of glasses on the basis of a spin- Hamiltonian equivalent to

$$H = g\mu_B \mathbf{BS} + D\left(S_z^2 - 35/12\right) + 1/2E\left(S_+^2 - S_-^2\right) \quad (1)$$

with $S = 5/2$ and $g = 2$. Here D and E are the axial and rhombic fs parameters. This Hamiltonian contains no quartic crystal field terms. An isotropic g of 30/7 from a high-spin (HS) d^5 ion in a site of rhombic symmetry can only appear if the symmetry is completely rhombic ($\lambda = E/D = 1/3$), making quartic crystal field terms are insignificant. Such interpretation was supported also by successful simulation of the spectra [14,15].

Less pronounced absorption in the EPR spectra of Fe (III)–PPA complex is observable at $g_{\text{eff}} = 6.7$. The case $\lambda = 0$, $D \neq 0$, corresponds to purely axial symmetry of the environment of the paramagnetic ions. This circumstance leads to highly anisotropic g-factor ($g_{\parallel\text{eff}} = 2$; $g_{\perp\text{eff}} = 6$), which was found for many high-spin ferric heme proteins [16,17]. Additionally, Fe^{3+} spectra in phosphate and borate glasses in which an additional absorption was observed in low magnetic field have been simulated using a fine-structure Gaussian distribution density by Yahiaoui et al. [14]. The agreement between the experimental and computer-simulated spectra suggests the existence, besides orthorhombic symmetry sites (with $\lambda = 1/3$), of a considerable number of Fe^{3+} sites with axial or weakly rhombic distortions ($\lambda \leqslant 0.08$). In this context, we think that features A and B (see Fig. 3) in EPR spectrum of Fe (III)–PPA complex are due to magnetically isolated HS Fe^{3+} ions in: (i) a completely rhombic and (ii) weakly rhombic environment, respectively. The insert in Fig. 3 shows the low-field peaks and simulation which was carried out using Hamiltonian (1) with the following parameters: $D = 0.5072$ T and $E = 0.2050$ T and software package used for studying polycrystalline powder.

The X-band spectrum of Fe (III)–PPA exhibits also resonance with $g_{\text{eff}} = 3.4$ (denoted as C—see Fig. 3). Golding et al. [13] considered a more general spin-Hamiltonian, in comparison with Eq. (1), with fourth-order terms for HS d^5 ions (Eq. (1) in [13]). They presented formulas for the energies and principal g-values, when the symmetry is tetragonal ($E = 0$) and $a \neq 0$ and $F \neq 0$. The conditions given by Golding are

$$g = 3.3 \quad \text{for} \quad 3D + 3a + F = 0; \quad E = 0$$
$$\text{and} \quad 3D + F = 0; \quad E = 0$$

and are fulfilled when the predominance of quartic fine-structure parameters in comparison with Zeeman term takes place. However, it is not observed in experiments (see discussion in [14]). Therefore, we explain the C feature in EPR spectrum of Fe (III)–PPA complex as assigned to Fe^{3+} in a strong crystal field environment. These low-spin (LS) ferric centres have been found in a number of heme proteins and small-molecule ferric porphyrin complexes [18–21] and are characterised by "large $g_{\max}$" EPR spectra with $g \geqslant 3.3$. This EPR spectral feature has been associated with "highly anisotropic low-spin (HALS)" species [20] and their presence is connected with the change of type and orientation of axial ligands. The observed intensity of this spectral feature is very temperature dependant what is shown in Fig. 4.

The broad line (denoted as D in Fig. 3) characterised with $g_{\text{eff}} = 2$ demonstrates that a fraction of the ferric ions in the sample is aggregated, i.e. the dipole–dipole and the exchange interactions between ferric ions are present. The magnetic properties of Fe (III)–pipem complex are represented in the form of the spin susceptibility versus T curves. In Fig. 5a, temperature evolution of EPR intensity, calculated as double integration of the spectrum of ferric complex is shown. The temperature dependence of the corresponding inverse intensity is illustrated in Fig. 5b. Additionally, in Fig. 5c and d, the intensity of components A and D (estimated as the product of peak-to-peak height and square of its width: $P = I_{\text{pp}}(\Delta B_{\text{pp}})^2$), is reported. This behaviour can be explained as follows: the dependence of inverse spin susceptibility in the range $3\,\text{K} \leqslant T \leqslant 300\,\text{K}$ is not linear as expected for a well-behaved paramagnet. With decreasing temperature the intensity of signal C decreases as well. It is known that the ferric ion in several materials [17,22,23] exhibits a thermally induced change of spin-state. The temperature dependence of the intensity of the $g_{\text{eff}} = 4.3$ line follows the Curie law, which means the absence of the exchange interaction between ferric ions contributing to A line. At the same time, it was established that the intensity of $g_{\text{eff}} = 2.0$ component follows the

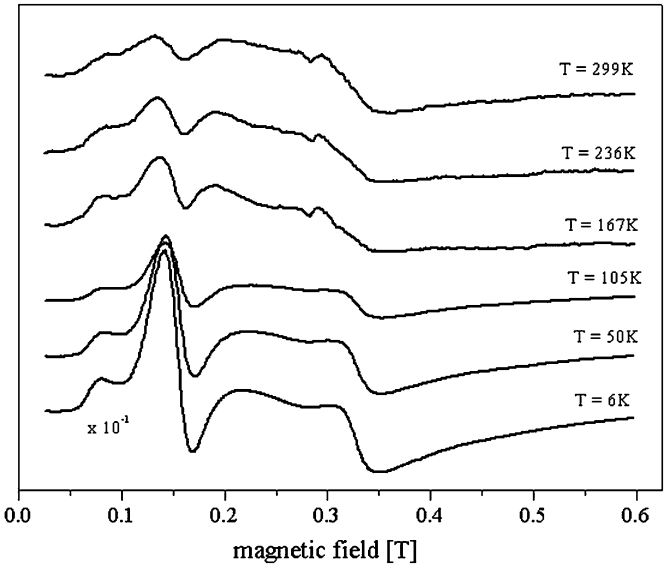

Fig. 4. The temperature evolution of the experimental EPR derivative spectra for the Fe (III)–PPA complex.

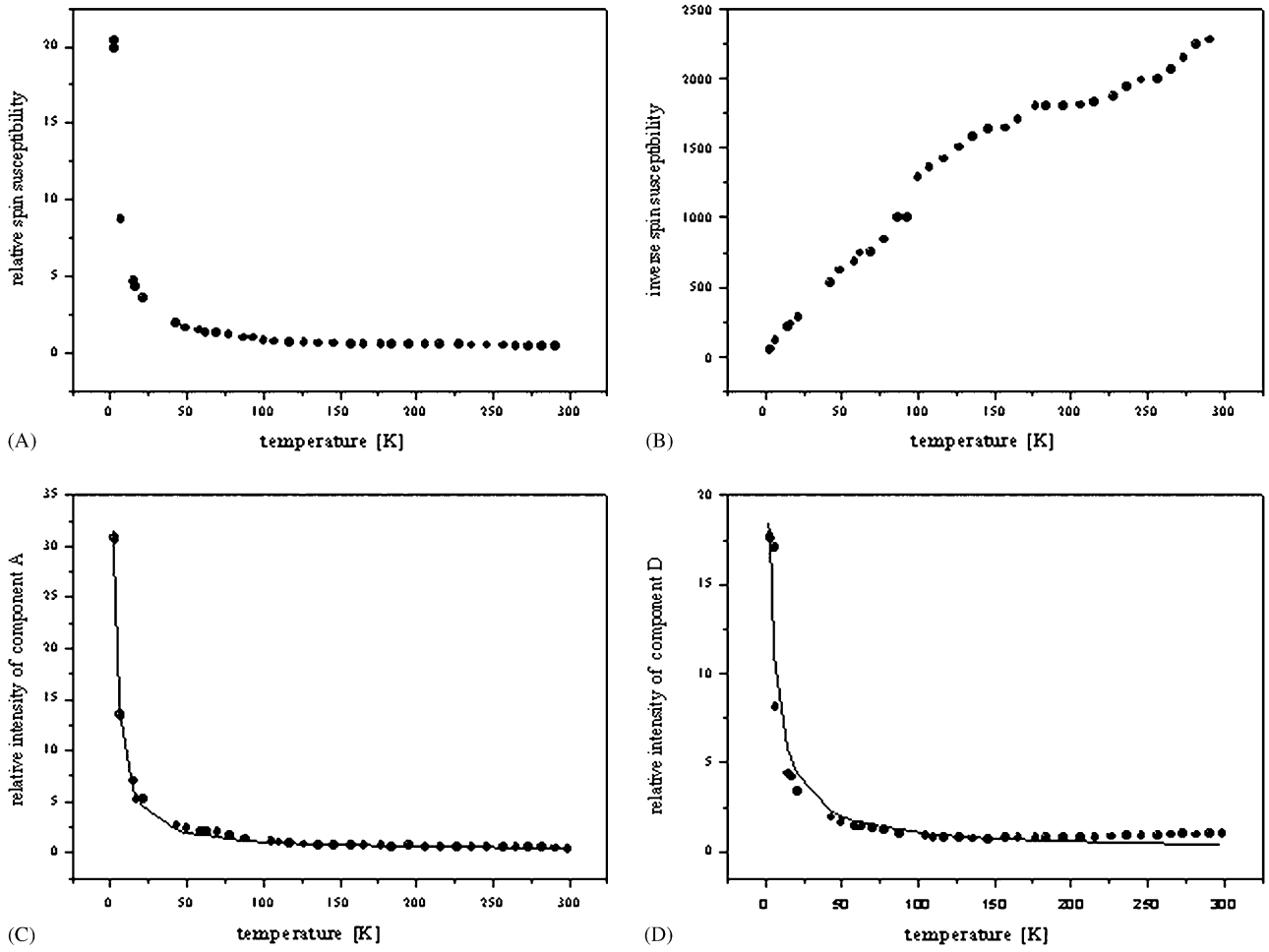

Fig. 5. The temperature evolution of EPR intensity for Fe (III)–PPA complex: (a) the plot of spin susceptibility vs. temperature calculated as double integration of the spectrum; (b) the temperature dependence of the corresponding inverse spin susceptibility; (c) and (d) the temperature dependence of the intensity of components A and D, respectively (estimated as the product of peak-to-peak height and square of its width: $P = I_{pp}(\Delta B_{pp})^2$). The solid line in (c) is calculated using Curie–Weiss law.

Curie–Weiss law with relatively weak exchange interactions. The small increase of this line at $T > 100$ K can be explained by the growth of the population of the levels of the spin multiplets at the high temperatures.

Concluding, the EPR investigations demonstrate that there are ferric ions in the Fe (III)–PPA complex in the different environments. The most of the paramagnetic centres, HS–Fe^{3+}, are located in the site of completely rhombic symmetry (line A). Besides, we observed the presence of HS ferric species in tetragonal local symmetry with the rhombic distortion (line B) and the LS ferric species in the rhombic symmetry (line C). It is also observed, that a fraction of the iron is aggregated (line D).

A number of the investigations by EPR technique of biologically important ferric complexes [18–21] show that Fe (III) may be characterised either as HS or LS states depending on the nature of the axial ligands. Besides, the characteristic features of disordered solids are distribution of the short-range order parameters, namely bond lengths and bond angles. For the confirmation of the proposition that iron (III) ions exhibit distorted octahedral configuration with the carbonyl and carboxylato oxygen atoms of the pipem and with oxygen atom of water molecule occupying the apical position, the XPS studies of investigated complex were carried out.

3.3. XPS studies

The XPS measurements were based on the 2p lines for iron and O1s, C1s, N1s lines in PPA and Fe–PPA complex. The spectra of these regions are shown in Figs. 7–11. The corresponding binding energy values are listed in Table 1.

Fig. 6 represents the XPS survey spectrum of the Fe (III)–PPA complex and clearly shows the presence of the chlorine atoms in the sample. We obtain the high-resolution spectrum of Cl2p signal with energy position at 198.5 eV. This value is characteristic for chlorine ions in $FeCl_3$ [24] Because of the chemical analysis excluded the presence of chlorine in the complex, we believe that Cl2p signal arises from residue of reagent. The Si2p signal visible in survey scan is descended from pipemidic acid.

Table 1
Core-level binding energies (eV) of N1s, C1s, O1s and Fe2p

Compound		N1s			C1s			O1s					Fe2p	
		C–N + H2–C	C = N–C	N(–C)3	C/H	C/N	C/O						$2p_{3/2}$*	$2p_{1/2}$*
								C = O		C–O		H_2O		
PPA	BE	398.1	399.7	401.2	284.5	286.2	288.6	531.0		532.2		533.4	—	—
	FWHM	2.3	2.3	2.3	3.0	2.6	2.6	2.3		1.9		2.1		
	% area[a]	20.0	40.0	40.0	23.0	61.5	15.4	50.0		25.0		25.0		
	% area[b]	19.6	41.0	39.3	21.4	64.2	14.3	45.7		26.7		27.6		
								C = O (b)	C = O	OH	C–O (b)	H_2O		
Fe(III)PPA	BE	399.0	400.0	401.5	284.5	286.2	288.6	530.1	531.2	532.0	532.5	533.8	711	724.8
	FWHM	2.3	2.3	2.3	2.5	2.3	2.3	1.8	1.8	1.8	1.8	1.8		
	% area[c]	20.0	40.0	40.0	23.0	61.5	15.4	16.7	16.7	33.3	16.7	16.7		
	% area[b]	19.5	41.6	39.0	20.0	65.1	14.8	16.7	16.7	33.3	16.7	16.7		

BE—binding energy; FWHM—full-width at half-maximum; (b)—bonded; *—maximal component.
[a]Calculated from molecular formula.
[b]Calculated from fitting of experimental signal.
[c]Calculated from proposed of molecular formula of Fe–PPA complex.

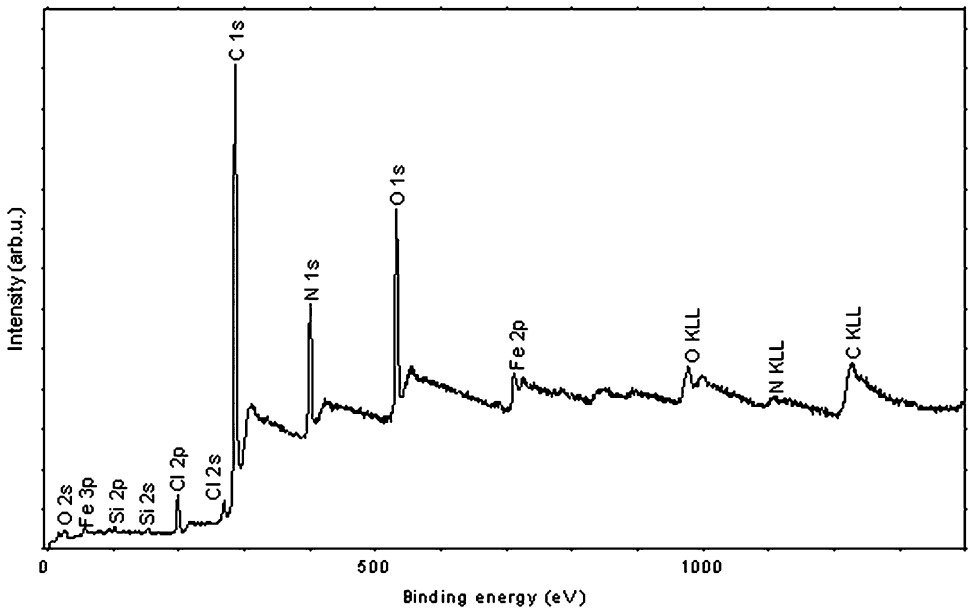

Fig. 6. The XPS survey spectrum of Fe (III)–PPA complex.

The Fe peak has complex structure (see Fig. 7) and this feature indicates that it is a composition of several contributions. One of the useful features of XPS spectroscopy is the shift in binding energy (BE) of core electrons of atoms in different chemical environments. These chemical shifts are associated with the effective charge on the atom from which the photoelectron originates. The BEs of several transition metal complexes have been reported by Feltham and Brant [25]. The results of these studies are that the metal BEs generally increase with the oxidation state of the metal and with the electron-withdrawing power of the ligand. Approximate values of BE for the transition metal in any complex, when the oxidation state of the central metal is constant and the coordination sphere differs, Feltham and Brant described as the following empirical rule:

$$\mathrm{MBE(eV)} = \sum_{\text{ligand}} \Delta M + N + M'(0),$$

where the first term is the summation over all ligand group shifts, N is the metal oxidation state and $M'(0)$ is the "bare" (uncharged and unligated) metal BE.

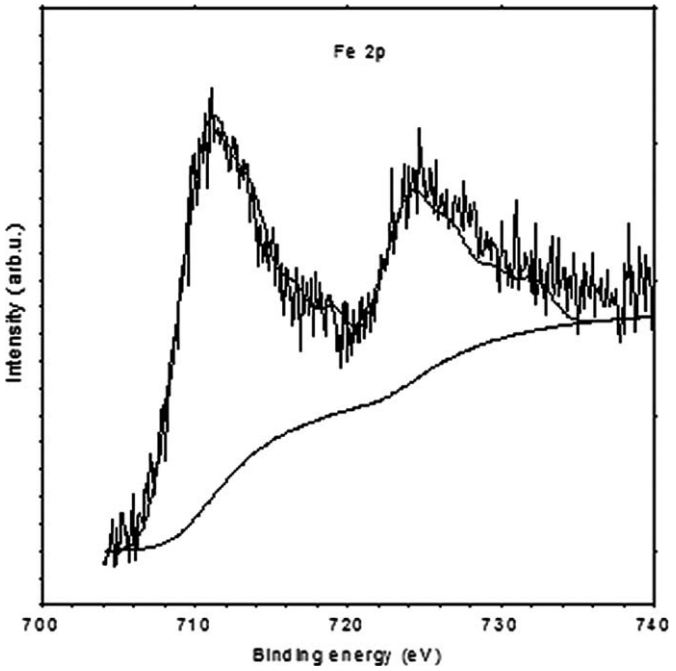

Fig. 7. The observed XPS spectrum of Fe2p for Fe (III)–PPA complex.

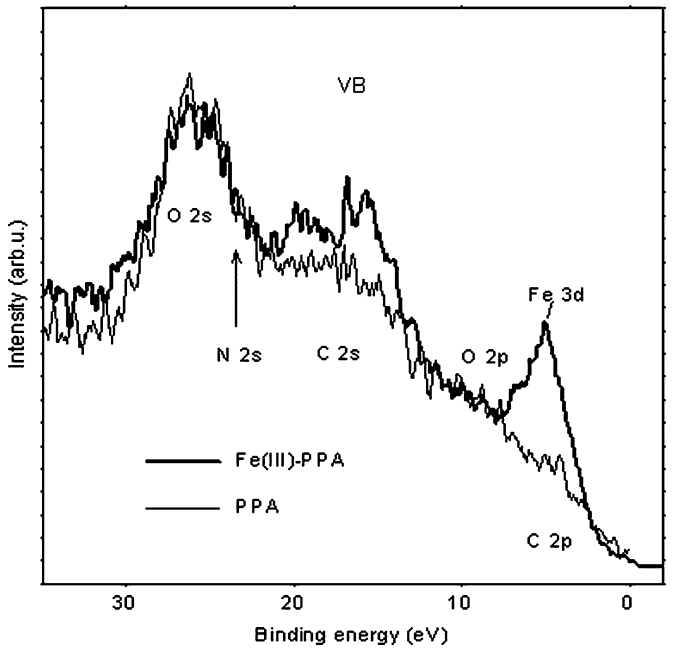

Fig. 8. The comparison of XPS VB of PPA and Fe (III)–PPA complex.

The empirically derived values for the ligand group shifts fall into two categories: negative value for σ-donor ligands (for example: for Cl: -0.5 eV) and positive shifts for π-acceptor ligands (for example: for C–O: $+0.6$ eV). Generally, these empirically derived values of the group shifts have a linear correlation with ligand electronegativity. In accordance with Fig. 7, the values of BE in maximum of $Fe2p_{3/2}$ and $Fe2p_{1/2}$ signals are typical for Fe (III). However, the shape of spectrum is the envelope of some components corresponding to different surroundings of iron and this result confirmed our conclusions from EPR investigations. Veal and Paulikas [26] showed the systematic dependence of energy separation between main line and satellites in XPS spectra of cation $2p_{3/2}$ levels versus ligand electronegativity (Pauling scale). In comparison with this data it was confirmed that iron cations are ligated to oxygen neighbours (energy separation is 8.4 eV in our case) [27].

The experimental valence-band spectra of PPA and Fe (III)–PPA complex are shown in Fig. 8. The sharp peak at the valence-band edge corresponds to excitation from the 3d level of the ferric ion. The satellite feature on the high binding energy side is very broad. This observation is clear in the light of calculations of theoretical valence-band of Fe_2O_3, which was done by Fujimori et al. [28]. These authors, using configuration-interaction theory based on a FeO_6-cluster model, explained VB structure as the multiplet structure of the mixed d^4, d^5L and d^6L^2 configurations.

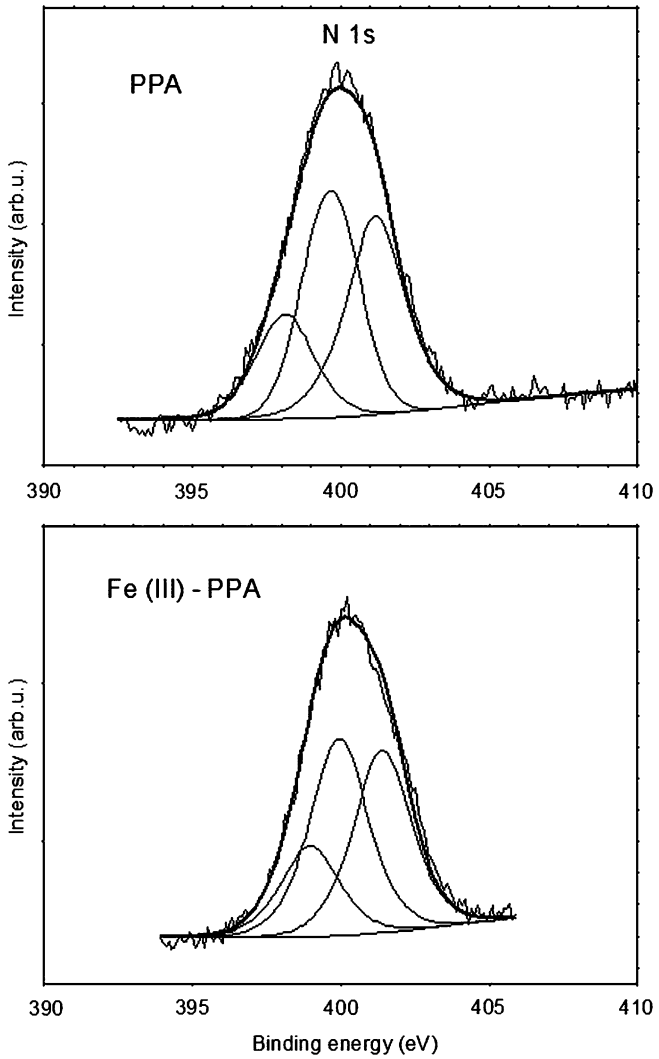

Fig. 9. The observed and deconvoluted XPS spectra of N1s for PPA and Fe (III)–PPA complex.

In Table 1, the core-level binding energies, FWHM and peak areas for pipemidic acid and its Fe (III) complex are shown. The XPS spectrum of N1s (Fig. 9) was deconvoluted into three components corresponding to three kinds of nitrogen in free ligand. The first one at binding energy 401.2 eV can be attributed to N(–C)3 bonding, second one at 399.7 eV to C═N–C bonding and third one at 398.1 eV to C–N + H2–C bonding [29,30]. The binding energy values change around 0.3 eV for the complex. This is indication that nitrogen is not directly bound to the metal ion. The greater chemical shift of last component is attributed to NH…O hydrogen bonds as results from IR studies.

In Fig. 10, the C1s spectra of PPA and Fe (III)–PPA are shown. The C1s signal was fitted to three components with the following contents: 21.4%, 64.2% and 14.3% corresponding to different surroundings of carbon. The main maximum has binding energy of 286.2 eV and corresponds to carbon in C–N group. The second and the third maxima (E_b^1C1s = 284.5 eV, E_b^3C1s = 288.6 eV) correspond to hydrocarbon and carbon connected with oxygen atoms, respectively [29]. These values are the same for free ligand and the complex.

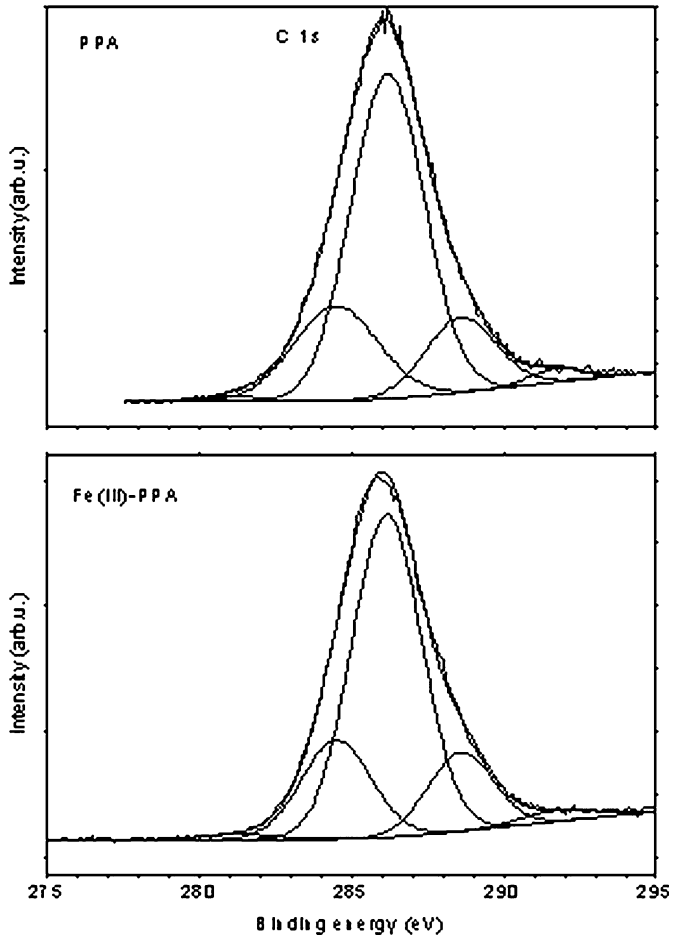

Fig. 10. The observed and deconvoluted XPS spectra of C1s for PPA and Fe (III)–PPA complex.

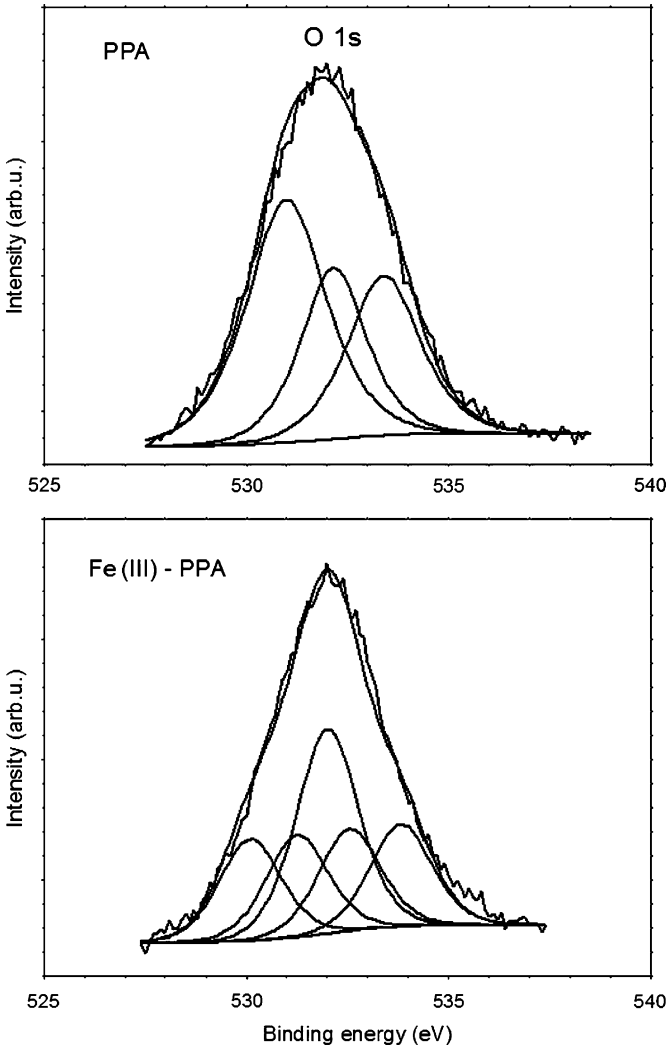

Fig. 11. The observed and deconvoluted XPS spectra of O1s for PPA and Fe (III)–PPA complex.

The XPS spectrum of O1s of PPA is shown in Fig. 11. A low energetical maximum defines bonds of C═O (E_b^1O1s = 531.0 eV), second maximum (E_b^2O1s = 532.2 eV) refers to bond of O–C [29] and third component (E_b^3O1s = 533.4 eV) is due to the presence of water molecules in free ligand [31,32]. In the Fe (III)–PPA complex, the spectrum was deconvoluted into five lines. On the basis of this fit and of the literature [32–37], we suggest the following assignment: the main peak at 532.0 eV is assigned to hydroxyl group OH–bonded to iron; the low energetical signals located at 530.1 and 531.2 eV correspond to two kinds of oxygen e.g. oxygen from carbonyl group no bonded to iron (531.2) as in the free ligand (Table 1) and oxygen from carbonyl group bonded to iron (530.1 eV); the signal at 532.5 eV can be identified as the bonded oxygen of C–O–Fe; the high energetical signal located at 533.8 eV is attributed to one bonded water molecule. These results corroborate the hypothesis about the proposed structure of the Fe (III)–PPA complex.

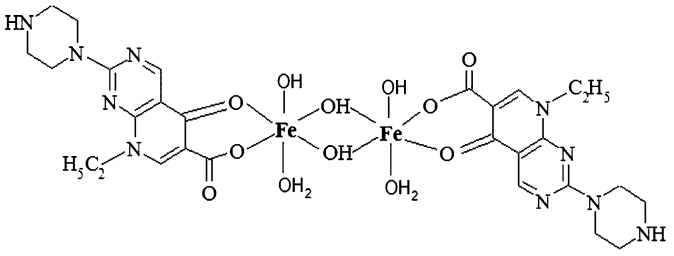

Fig. 12. The proposed structure of the dimeric iron (III) complex of pipemidic acid.

4. Conclusions

The EPR and XPS study of Fe (III) complex of pipemidic acid leads to the following conclusions:

- The character of the spectroscopic spectrum is determined by a poor crystallisation of the sample:
  (a) the observed EPR spectrum consists of several components. The complexity of the EPR spectra for examined Fe (III)–pipem complex results from extreme sensitivity to geometry of iron (III) chromophore. Therefore, it is directly connected with the crystallinity of this compound. Additionally, the thermally induced change of spin-state of Fe (III) ions was observed.
  (b) FWHM of XPS components is up to 2.6 eV.
  They are characteristic features of disordered solids namely, distribution of the short-range order parameters: bond lengths and bond angles.
  It is worth noting that title compound—iron (Fe)–pipemidic acid (PPA) complex—is a novel material and the first time is characterised. Our attempts to produce the single crystals of obtained Fe–PPA complex have unfortunately failed because of a weak solubility of the compounds.
- The EPR and XPS results confirm the optical spectroscopic and elemental analysis conclusions that iron cations are bonded to oxygen neighbours.
- In Fig. 12 is shown the tentative structure of Fe (III) complex of pipemidic acid. Six coordinate dimer distorted octahedral configuration has been proposed for [Fe (pipem) $(HO)_2$ $(H_2O)]_2$.

References

[1] I. Fonseca, S. Martinez-Carrera, S. Garcia-Blanco, Acta Cryst. 42 (1986) 1618.
[2] L. Yang, D. Tao, X. Yang, Y. Li, Y. Guo, Chem. Pharm. Bull. 51 (5) (2003) 494–498 and references therein.
[3] P.T. Lieu, M. Heiskala, P.A. Peterson, Y. Yang, Mol. Asp. Med. 22 (2001) 1–87.
[4] I. Turel, Coord. Chem. Rev. 232 (2002) 27–47 and references therein.
[5] D. Kovala-Demertzi, J. Inorg. Biochem. 79 (2000) 153.
[6] B. Szymanska, D. Skrzypek, D. Kovala-Demertzi, M. Staninska, M.A. Demertzis, Spectrochim. Acta Part A 63 (2006) 518–523.
[7] J.F. Moulder, W.F. Stickle, P.E. Sobol, K.D. Bomben, Handbook of X-ray Photoelectron Spectroscopy Physical Electronic, Physical Electronic Inc., 1995.
[8] D. Kovala-Demertzi, A. Galani, M.A. Demertzis, S. Skoulika, C. Kotoglou, J. Inorg. Biochem. 98 (2004) 358.
[9] V. Dokorou, M.A. Demertzis, J.P. Jasinski, D. Kovala-Demertzi, J. Organomet. Chem. 689 (2004) 317.
[10] J. Kliava, Phys. Stat. Solidi (b) 134 (1986) 411–455.
[11] T.D. Smith, J.R. Pilbrow, in: L.J. Berliner, J. Reuben (Eds.), Biological Magnetic Resonance, vol. 2, Plenum Press, New York and London, 1980, pp. 85–168 and references therein.
[12] R. Cammack, C.E. Cooper, Methods Enzymol. 227 (1993) 353–384.
[13] R.M. Golding, T. Singhasuwich, W.C. Tennant, Mol. Phys. 34 (1977) 1343–1350 and references therein;
D.G. McGavin, W.C. Tennant, Mol. Phys. 45 (1982) 77–86.
[14] E.M. Yahiaoui, R. Berger, Y. Servant, J. Kliava, L. Cugunov, A. Mednis, J. Phys.: Condens. Matter 6 (1994) 9415–9428.
[15] J. Kliava, R. Berger, Mol. Phys. Rep. 39 (2004) 130–136.
[16] W.E. Blumberg, Methods Enzymol. 76 (1981) 312–329.
[17] F.A. Walker, in: K.M. Kadish, K.M. Smith, R. Guilard (Eds.), The Porphyrin Handbook, vol. 5, Academic Press, New York, 2000, pp. 81–183 and references therein.
[18] J.C. Salerno, J.S. Leigh, J. Am. Chem. Soc. 106 (1984) 2156–2159.
[19] F.A. Walker, B.H. Huynh, W.R. Scheidt, S.R. Osvath, J. Am. Chem. Soc. 108 (1986) 5288–5297.
[20] D. Inniss, S.M. Soltis, C.E. Strouse, J. Am. Chem. Soc. 110 (1988) 5644–5650.
[21] F.A. Walker, Coor. Chem. Rev. 185–186 (1999) 471–534 and references therein.
[22] Y.V. Yablokov, V.V. Zelentsov, M. Augustyniak-Jablokow, A. Krupska, J. Mrozinski, Mater. Sci. 21 (2003) 215–223.
[23] D. Skrzypek, I. Madejska, J. Habdas, J. Phys. Chem. Sol. 66 (2005) 91–97.
[24] K.L. Tan, B.T.G. Tan, E.T. Kang, K.G. Neoh, Y.K. Ong, Phys. Rev. 42 (1990-) 7563–7566.
[25] R.D. Feltham, P. Brant, J. Am. Chem. Soc. 104 (1982) 641–645.
[26] B.W. Veal, A.P. Paulikas, Phys. Rev. B 31 (1985) 5399–5416.
[27] M. Descostes, F. Mercier, N. Thromat, C. Beaucaire, M. Gautier-Soyer, Appl. Surf. Sci. 165 (2000) 288–302.
[28] A. Fujimori, M. Saeki, N. Kimizuka, M. Taniguchi, S. Suga, Phys. Rev. B 34 (1986) 7318–7328.
[29] Beamson, Briggs, High Resolution XPS of Organic Polymers—The Scienta ESCA 300 Database, Wiley, Chichester, 1992.
[30] R. Ohta, K.H. Lee, N. Saito, Y. Inoue, H. Sugimura, O. Takai, Thin Solid Films 434 (2003) 296–302.
[31] G.B. Hoflund, W.S. Epling, D.M. Minahan, J. Electron. Spect. Rel. Phen. 95 (1998) 289–297.
[32] F. Grellner, B. Klingenberg, D. Borgmann, G. Wedler, J. Electron. Spect. Rel. Phen. 71 (1995) 107–115.
[33] D. Atzei, C. Sadun, L. Pandolfi, Spectrochim. Acta A 56 (2000) 531–540.
[34] D. Atzei, A. Rossi, C. Sadun, Spectrochim. Acta A 56 (2000) 1875–1886.
[35] V. Bondarenka, S. Grebinskij, S. Kaciulis, G. Mattogno, S. Mickevicius, H. Tvardauskas, V. Volkov, G. Zakharova, J. Electron. Rel. Phen. 120 (2001) 131–135.
[36] V.I. Kodolov, E.I. Tchirkova, S.G. Bystrova, I.N. Shabanova, O.V. Popova, S.N. Babushkina, J. Electron. Spect. Rel. Phen 88–91 (1998) 977–982.
[37] C. Lamonier, A. Bennani, A. D'Huysser, A. Aboukais, G. Wrobel, J. Chem.Soc., Faraday Trans. 92 (1996) 131–136.